

Article

# Influence of Graphene Oxide on Rheological Parameters of Cement Slurries

Marcin Kremieniewski 

Oil and Gas Institute—National Research Institute, 25A Lubicz Str., 31-503 Krakow, Poland; marcin.kremieniewski@inig.pl or kremieniewski@inig.pl

Received: 23 September 2020; Accepted: 15 October 2020; Published: 19 October 2020



**Abstract:** In recent years, graphene-based nanomaterials have been increasingly and widely used in numerous industrial sectors. In the drilling industry, graphene oxide in cement slurry has significantly improved the mechanical parameters of cement composites and is a future-proof solution. However, prior to placing it in a borehole ring space, cement slurry must feature appropriate fluidity. Graphene oxide has a significant influence on rheological parameters. Therefore, it is necessary to study graphene oxide's influence on the rheological parameters of cement slurries. Thus, this paper presents rheological models and the results of studies on rheological parameters. A basic cement slurry and a slurry with a latex addition were used. The latex admixture was applied at concentrations of 0.1%, 0.03%, and 0.06%. In total, studies were carried out for six slurries with graphene oxide and two basic slurries. The obtained results of studies on the slurries with graphene oxide were compared with the control slurry. It was found that the smallest graphene oxide concentration increased slurry value, some rheological parameter values, plastic viscosity, and the flow limit. Surprisingly, a concentration up to 0.03% was an acceptable value, since the increase in plastic viscosity was not excessively high, which allowed the use of cement slurry to seal the hole. Once this value was exceeded, the slurry caused problems at its injection to the borehole.

**Keywords:** cement slurry; graphene; graphene oxide (GO); nanotubes; rheological parameters; plastic viscosity; yield strength; structural strength; advanced drilling solution

## 1. Introduction

New allotropic varieties of carbon, such as nanostructural varieties (i.e., fullerenes and carbon nanotubes (CNT)), are a breakthrough for many industrial sectors. Modifying cement slurries with the use of carbon nanotubes is ongoing in the oil sector. These are rolled-up graphene planes. Their structure features a closed surface because nanotubes are finished on one or both ends with semicircular caps [1–5]. Carbon nanotubes feature a large specific surface, new and changed electron properties, and a high Young's modulus that reaches 2 TPa. Very strong bonds exist between carbon atoms, which substantially increase graphene strength. This contributes to very high values of the tensile strength (up to 50 GPa). Carbon nanotubes have high bending strength and good conductivity of heat and electric currents. The diameter of the nanotubes most frequently varies between 1 and 100 nm with a length between 10 nm and 2–10  $\mu$ m [6–11]. Certain studies [12–16] have confirmed that the application of carbon nanotubes substantially improves the nano- and micromechanical parameters of cement slurries. An increase in the crack resistance of the cement matrix and local stiffness of the CSH phase during nanohardness testing is an important feature. As a result of these obtained parameters, slurries with graphene provide an advanced drilling solution for borehole sealing. Cement slurry modification by means of a graphene admixture causes a decrease of the set cement porosity and an increase in the compressive strength of cement composites [17–21]. In studies that used a scanning electron microscope (SEM), it was found that the use of graphene in cement slurry caused the formation of bridges between

nano- and microscratches in the binder [21,22]. This resulted in an increased tensile strength and the further propagation of scratches, which was also confirmed in the literature [5,23–27]. However, other papers have provided contradictory information on the influence of nanotubes on the mechanical parameters of cement slurries. The authors of [28–30] compared the variable results of slurry mechanical properties tests, in which a nanoadditive was applied. Furthermore, they summarized the application of carbon nanotubes in concrete technology. Some of the discussed studies confirmed an improvement in parameters such as compressive strength or the Young's modulus. However, other studies showed the deterioration of those features [31,32]. Economic factors present a major obstacle in the application of nanotubes. Nanotubes feature poor adhesion to set cement. In addition, they agglomerate and are unevenly distributed in cement slurry. Therefore, modifying cement slurry via a graphene mesh was studied. This is a cheaper material with high mechanical strength. Compared to nanotubes, it does not reveal the aggregation of individual structures, which eliminates the issue of inhomogeneous arrangement in the slurry. Graphene oxide, which is a graphene derivative, has average mechanical properties that are parallel to possible material homogenization in the cement slurry. The concentration of 0.01–0.05% of graphene oxide compared to cement weight can reduce slurry porosity, accelerate the initial hydration process, and increase the values of mechanical parameters. Recent studies [18,31–35] have described the positive influence of graphene oxide on the mechanical properties of cement slurry. This is due to a reaction occurring between  $\text{Ca}^{2+}$  ions present in the hydrating slurry with -COOH groups on the edges of graphene oxide nanoflakes. The reaction results in a compact strengthened spatial structure that consists of cement and graphene oxide nanoflake hydration products [36,37].

Such a positive influence of graphene oxide on mechanical and structural parameters is invaluable in cement slurry technology. However, previous research was carried out mainly from the point of view of hardened cement slurry [38–42]. Prior to borehole pumping, cement slurry is a rheo-unstable liquid. During the performance of sealing and strengthening rock mass via drilling technologies, the rheological properties of cement slurry are the main parameters that decide the success of cementing operations.

When analyzing the available literature, no papers were related to the rheological parameters of slurries modified with graphene oxide. Therefore, this paper is aimed at supplementing the deficit with the results of other studies.

The rheological parameters of cement slurries are crucial during the design and execution of works related to the sealing and strengthening of soil or rock mass [7,43–45]. Their appropriate choice contributes to ensuring the required tightness in the borehole. Obtaining the required rheological parameters is related to the selection of a rheological model, which can determine its parameters [43]. The rheological properties of cement slurries are the subject of interest because they show a relationship with:

- ✓ Course of the slurry setting process;
- ✓ Consistency;
- ✓ Stability;
- ✓ Selection of the technology for slurry injection into the sealed environment;
- ✓ Resistance to the slurry flow through the circulation system [43].

The dispersion system to which the cement slurry belongs is extremely complex. This results from the fact that rheology is significantly affected by hydration reactions occurring in the slurry versus time [10,43,44,46]. The presence of nanomaterials or other modifying admixtures is an additional factor that affects the slurry's rheological variability. It should be emphasized that cement slurries may feature various rheological properties depending on the time of measurement after slurry preparation. Flow curves may be reversible or show hysteresis. This results from the fact that, at short measurement times, the slurry's structural damage dominates, while at longer times, the slurry's reconstruction prevails. In drilling fluid technology, rheological models are used to describe causalities that exist between rheological parameters and the technology of their application [44,47–52]. Based on the rheological model matching real fluid behavior, it is possible to reduce the errors of the calculated quantities, i.e.,

flow character, fluid flow resistance in the circulation system, and particle sedimentation [44,53–57]. Depending on the type of fluid, various mathematical formulas describing its behavior during flow were used [43,58–62]. These are mainly relationships between the shear rate and shear stress [43].

Newton

$$\tau = \eta \left( -\frac{dv}{dr} \right) \quad (1)$$

Bingham

$$\tau = \tau_y + \eta_{pl} \left( -\frac{dv}{dr} \right) \quad (2)$$

Casson

$$\sqrt{\tau} = \sqrt{\tau_y} + \sqrt{\eta_{cos}} \cdot \sqrt{\left( -\frac{dv}{dr} \right)} \quad (3)$$

Herschel–Bulkley

$$\tau = \tau_y + k \left( -\frac{dv}{dr} \right)^n \quad (4)$$

Ostwald–de Waele

$$\tau = k \left( -\frac{dv}{dr} \right)^n \quad (5)$$

There are also relationships between the shear rate or shear stress and apparent viscosities (2010):

Carreau–Yasuda

$$\frac{\eta - \eta_\infty}{\eta_0 - \eta_\infty} = \left[ 1 + \left( \lambda \left( -\frac{dv}{dr} \right)^a \right)^{\frac{n-1}{a}} \right] \quad (6)$$

Cross

$$\frac{\eta - \eta_\infty}{\eta_0 - \eta_\infty} = \frac{1}{\left( 1 + \lambda \left( -\frac{dv}{dr} \right) \right)} \quad (7)$$

Ellis

$$\eta = \frac{\eta_0}{1 + \left( \frac{\tau}{\tau_2} \right)^{\alpha-1}} \quad (8)$$

Krieger–Dougherty

$$\eta_r = \left( 1 - \frac{\Phi}{\Phi_m} \right)^{-[\eta]\Phi_m} \quad (9)$$

Meter

$$\eta = \eta_\infty + \frac{\eta_0 - \eta_\infty}{1 + \left( \frac{\tau}{\tau_2} \right)^{\alpha-1}} \quad (10)$$

Powell–Eyring

$$\eta = \eta_\infty + (\eta_0 - \eta_\infty) \frac{\sinh^{-1} \left( \lambda \left( -\frac{dv}{dr} \right) \right)}{\lambda \left( -\frac{dv}{dr} \right)} \quad (11)$$

where:

$\tau$ —shear stress;

$\tau_y$ —yield stress;

$dv/dr$ —shear rate gradient;

$\eta$ —viscosity;

$\eta_{pl}$ —plastic viscosity;

$\eta_0$ —zero viscosity;

$\eta_\infty$ —viscosity at the shear rate approaching infinity;

$k$ —coefficient of consistency;

$n$ —exponent;

$\Phi$ —degree of particles packing for the Krieger–Daugherty model;

$\Phi_m$ —maximum degree of packing for the Krieger–Daugherty particles;

$\lambda$ —time constant.

When studying the rheological parameters of cement slurries, which are complicated dispersion systems, experiments must be carried out at a wide range of shear rates [10,43,44,63–69]. Therefore, the studies were performed using a rotational viscometer at a shear rate that ranged from  $1022\text{ s}^{-1}$  to  $1.70\text{ s}^{-1}$ . Slurries modified with a graphene oxide admixture featured higher values of mechanical parameters. However, the presence of graphene oxide affected rheological parameters. Therefore, the influence of graphene oxide on the rheological parameters of cement slurries was studied. The optimum rheological model of cement slurries was chosen as a result of rheological curve determination, enabling the best description of measurement results in the shear stress ( $\tau$ )–shear rate ( $\dot{\gamma}$ ) system of coordinates. Rheological parameters for individual models were determined using the method of regression analysis. The optimum rheological model for the slurry with the studied graphene oxide concentration was determined based on statistical tests [10,44].

## 2. Materials and Methods

### 2.1. Materials

CEM I 42.5R Portland cement was used to prepare the slurries. The cement contained 3.22% of  $\text{SO}_3$  and 0.069% of  $\text{Cl}^-$ . The specific surface of the cement was  $3426\text{ cm}^2/\text{g}$ , specific density was  $3.09\text{ g/cm}^3$ , and the alkali content was (eq.  $\text{Na}_2\text{O}$ ) 0.61%. The tap water contained 0.064 mg/L  $\text{NH}_4$  of ammonia, 2.95 mg/L  $\text{NO}_3$  of nitrates, 0.048 mg/L  $\text{NO}_2$  of nitrites, 29.2  $\mu\text{g/L}$  Fe of iron, 5.81  $\mu\text{g/L}$  Mn of manganese, and 344.0 mg/L  $\text{CaCO}_3$  of calcium carbonate. The graphene oxide used to prepare slurries was an oxidized form of graphene. This form was created in the process of graphene crystal oxidation with a mixture of sulfuric acid, sodium nitrate, and potassium permanganate (Hummers' method). From a molecular structure point of view, graphene oxide resembles a honeycomb with additional groups containing oxygen. Because of the high affinity of those groups with water molecules, the graphene oxide was hydrophilic and water-soluble. The graphene oxide contained 79% of carbon and 20% of oxygen. The flake size was 0.5–5  $\mu\text{m}$  and the thickness (minimum 80% of flakes) was one atomic layer. Centrifugation was used to prepare large flakes at a high concentration. Ultrahighly concentrated graphene oxide adopted sheet-like forms. The graphene oxide used was purchased from the company Graphene Supermarket, USA. To eliminate microflows of gas, latex was used in the drilling sector, which was an aqueous dispersion of a styrene-butadiene copolymer. The latex used was purchased from Polski Serwis Płynów Wiertniczych Sp. z o.o.

### 2.2. Slurry Preparation

In total, eight recipes were prepared to determine the influence of graphene oxide on the rheological parameters of cement slurries. Slurries 1–4 were pure slurries and Slurries 5–8 were slurries with a latex addition. The first slurry was a control sample. Samples 2 to 4 were slurries modified with a graphene oxide admixture of 0.01%, 0.03%, and 0.06%, respectively. The same scheme was used in the slurries with a 2.5% latex admixture. Slurry 5 was a control sample, whereas Slurries 6–8 contained graphene oxide at amounts of 0.01% to 0.06%. The latex and graphene oxide concentration was taken against the batch water amount (BWOC).

At the slurry preparation, a defined amount of water was measured via a graduated cylinder. An appropriate amount of graphene oxide aqueous dispersion was batched into the water. In the second group of slurries, latex was batched into the water. Water with a graphene addition was poured into a mixer. The rotational speed was set to 1600 rpm and the mixing lasted 10 min. After that time, the cement was poured into the batched water blend and the mixing continued for another 20 min. The mixing procedure at a low rotational speed reflected the slurry preparation under borehole

conditions. The basic slurry, marked as No. 1 in Table 1, was prepared first. The water–cement coefficient of the slurry was 0.50. In the next slurries, graphene oxide at planned amounts was introduced.

**Table 1.** Compositions of studied cement slurries.

Composition	Action	No. 1	No. 2	No. 3	No. 4	No. 5	No. 6	No. 7	No. 8
Water–cement ratio		0.46	0.46	0.46	0.46	0.46	0.46	0.46	0.46
Latex	Cement matrix sealing	0.0	0.0	0.0	0.0	2.5	2.5	2.5	2.5
Graphene	Mechanical parameters improvement	0.0	0.01	0.03	0.06	0.0	0.01	0.03	0.06
CEM I 42.5R Cement	Sets the cement slurry	100.0	100.0	100.0	100.0	100.0	100.0	100.0	100.0

Graphene in % by mass of cement.

### 2.3. Experimental Procedures

The studies on rheological properties were carried out based on shear curve determination. Tests were performed for 12 rotational speeds: 600, 300, 200, 100, 60, 30, 20, 10, 6, 3, 2, and 1 rpm, corresponding to the following shear rates ( $\dot{\gamma}$ ): 1022, 511.2, 340.8, 170.4, 102.2, 51.1, 34.08, 17.04, 10.22, 4.11, 3.41, and  $1.70 \text{ s}^{-1}$ . Studies were carried out at  $20 \text{ }^\circ\text{C} \pm 2 \text{ }^\circ\text{C}$ . The tap water, deprived of any mechanical pollution, was batched liquid. An OFITE 900 viscometer with coaxial cylinders was used in the rheological properties' studies. Numerical software "Rheo Solution" was used to facilitate computations related to the determination of optimum rheological models for the studied slurries. This software is owned by the Faculty of Drilling, Oil and Gas of the AGH University of Science and Technology and is used in other scientific and research work. The laboratory studies were aimed at determining the influence of graphene oxide on rheological parameters of cement slurries.

Tables 2–5 present the calculated rheological parameters of cement slurries with different concentrations of graphene oxide. Rheological parameters were calculated for the following models [10,35,46,52]:

- Newton;
- Bingham;
- Casson;
- Ostwald–de Waele;
- Herschel–Bulkley.

**Table 2.** Parameters of selected rheological models for slurries prepared with graphene oxide without a latex admixture.

Rheological Model	Rheological Parameters	Composition No.			
		1	2	3	4
Newtonian	Newton's dynamic viscosity, Pa·s	0.0935	0.0993	0.1097	0.1306
	Correlation coefficient, -	0.0000	0.0000	0.0000	0.0000
Bingham	Plastic viscosity, Pa·s	0.0600	0.0636	0.0712	0.0766
	Flow limit, Pa	21.6059	23.0592	24.9136	34.9151
	Correlation coefficient, -	0.8854	0.8899	0.9096	0.8353
Ostwald–de Waele	Coefficient of consistency, Pa·s <sup>5</sup>	7.4090	8.1303	9.4095	12.6893
	Exponent, -	0.3421	0.3363	0.3240	0.3152
	Correlation coefficient, -	0.9831	0.9857	0.9906	0.9628
Casson	Casson's viscosity, Pa·s	0.0318	0.0331	0.0358	0.0379
	Flow limit, Pa	13.2941	14.3810	15.8959	22.6342
	Correlation coefficient, -	0.9344	0.9386	0.9537	0.8978
Herschel–Bulkley	Flow limit, Pa	13.3732	13.7834	14.1473	31.3900
	Coefficient of consistency, Pa·s <sup>n</sup>	19.0041	19.3433	22.9940	37.2710
	Exponent, -	0.2168	0.2208	0.2779	0.1028
	Correlation coefficient, -	0.9926	0.9937	0.9922	0.9885
Apparent viscosity at 1022.04, s <sup>-1</sup> , Pa·s		0.072	0.077	0.087	0.098

**Table 3.** Parameters of selected rheological models for slurries prepared with graphene oxide containing a latex admixture.

Rheological Model	Rheological Parameters	Composition No.			
		5	6	7	8
Newtonian	Newton's dynamic viscosity, Pa·s	0.0682	0.0743	0.0967	0.1664
	Correlation coefficient, -	0.000	0.0000	0.0000	0.0000
Bingham	Plastic viscosity, Pa·s	0.0409	0.0392	0.0431	0.0993
	Flow limit, Pa	17.6483	22.7031	34.6101	43.3617
	Correlation coefficient, -	0.9672	0.9397	0.9036	0.9268
Ostwald–de Waele	Coefficient of consistency, Pa·s <sup>5</sup>	10.1599	13.6580	21.5698	22.3456
	Exponent, -	0.2176	0.1912	0.1599	0.2500
	Correlation coefficient, -	0.9535	0.9703	0.9797	0.9929
Casson	Casson's viscosity, Pa·s	0.0116	0.0125	0.0147	0.0410
	Flow limit, Pa	13.5152	18.0410	28.7196	31.1932
	Correlation coefficient, -	0.9891	0.9771	0.9592	0.9735
Herschel–Bulkley	Flow limit, Pa	13.4668	13.6058	14.3889	22.6583
	Coefficient of consistency, Pa·s <sup>n</sup>	0.7647	2.4951	11.0039	14.9704
	Exponent, -	0.5779	0.4096	0.2555	0.3392
	Correlation coefficient, -	0.9870	0.9838	0.9827	0.9962
Apparent viscosity at 1022.04, s <sup>-1</sup> , Pa·s		0.056	0.058	0.072	0.130

**Table 4.** Results of measurements and calculated values of apparent viscosity for slurries with graphene oxide without a latex admixture.

Shear Rate, s <sup>-1</sup>	Shear Stress, Pa				Apparent Viscosity, Pa·s			
	Composition No.				Composition No.			
	1	2	3	4	5	6	7	8
1.703	9.7090	11.242	13.797	16.863	5.700	6.600	8.100	9.900
3.407	9.7090	9.7090	10.731	13.797	2.850	2.850	3.150	4.050
5.110	10.220	12.264	15.330	21.462	2.000	2.400	3.000	4.200
10.220	15.841	17.374	18.907	21.973	1.550	1.700	1.850	2.150
17.034	21.462	21.973	22.995	33.215	1.260	1.290	1.350	1.950
34.068	31.682	32.193	34.237	47.012	0.930	0.945	1.005	1.380
51.102	34.237	36.281	39.858	57.743	0.670	0.710	0.780	1.130
102.204	37.814	41.391	44.457	61.320	0.370	0.405	0.435	0.600
170.340	41.391	45.479	47.523	64.897	0.243	0.267	0.279	0.381
340.680	51.100	54.166	57.743	74.095	0.150	0.159	0.169	0.217
511.020	58.765	59.787	65.919	80.227	0.115	0.117	0.129	0.157
1022.040	73.584	79.205	88.914	100.156	0.072	0.077	0.087	0.098

**Table 5.** Results of measurements and calculated values of apparent viscosity for slurries with graphene oxide containing a latex admixture.

Shear Rate, s <sup>-1</sup>	Shear Stress, Pa				Apparent Viscosity, Pa·s			
	Composition No.				Composition No.			
	1	2	3	4	5	6	7	8
1.703	12.775	16.863	26.061	28.105	7.500	9.900	15.299	16.499
3.407	12.775	16.352	26.061	28.616	3.750	4.800	7.650	8.400
5.110	13.797	16.863	27.083	30.149	2.700	3.300	5.300	5.900
10.220	16.863	21.462	31.171	36.792	1.650	2.100	3.050	3.600
17.034	20.951	26.061	37.303	42.413	1.230	1.530	2.190	2.490
34.068	22.484	28.616	41.902	53.144	0.660	0.840	1.230	1.560
51.102	22.484	28.616	43.946	58.765	0.440	0.560	0.860	1.150
102.204	24.528	30.149	45.99	68.985	0.240	0.295	0.450	0.675
170.340	27.083	32.704	48.545	76.139	0.159	0.192	0.285	0.447
340.680	34.237	39.347	53.655	88.403	0.100	0.115	0.157	0.259
511.020	39.347	44.968	58.765	101.178	0.077	0.088	0.115	0.198
1022.040	57.232	59.276	74.095	132.86	0.056	0.058	0.072	0.130

For each of the analyzed cement slurries, a rheological model was adopted, which featured the highest value of the correlation coefficient.

### 3. Results and Discussion

To determine the influence of graphene oxide on the rheological parameters of cement slurries, the measurements were carried out with shear rates as large as possible (up to  $1022 \text{ s}^{-1}$ ). Parameters corresponding to a specific rheological model were calculated from the obtained results. In addition, a slurry flow curve was prepared (Figure 1). As Tables 2 and 3 show, the studied slurries were non-Newtonian fluids. They were described by the Casson and Herschel–Bulkley models, for which the highest correlation coefficient occurred (from sample No. 4, 0.8978, the Casson model, to sample No. 8, 0.9962, the Herschel–Bulkley model). These two rheological models were mainly analyzed during the interpretation stage. The other models were compared for information purposes. As Table 2 shows, the basic slurry without the addition of latex, marked as No. 1, featured a plastic viscosity $_{C_{SS}}$  of 0.0318 Pa·s. The flow limit $_{HB}$  of this slurry was 13.37 Pa and the coefficient of consistency $_{HB}$  was  $19.0041 \text{ Pa}\cdot\text{s}^n$ . The apparent viscosity was 0.072 Pa·s. As Figure 1 shows, the flow curve for this slurry featured the lowest course. Moreover, on the graph of apparent viscosity change versus shear rate (Figure 2), the curve for basic slurry No. 1 featured the lowest course. Slurry No. 2 contained the smallest graphene oxide concentration of 0.01%. This slurry featured a higher viscosity $_{C_{SS}}$  than the basic slurry, equal to 0.0331 Pa·s. As Table 3 shows, the flow limit $_{HB}$  of slurry No. 2 was 13.78 Pa and the coefficient of consistency $_{HB}$  was  $19.3433 \text{ Pa}\cdot\text{s}^n$ . The apparent viscosity of this slurry slightly increased against the control recipe No. 1 and was 0.077 Pa·s (Table 2). The flow curve of sample No. 2 (Figure 1) was situated much higher than control slurry No. 1, proving that the slurry was thickened by a 0.01% graphene oxide (GO) concentration. When comparing changes of apparent viscosity versus the shear rate (Figure 2), the curve for slurry No. 2 was situated much higher than the sample without GO. The further increase in graphene oxide concentration in slurries Nos. 3 and 4 increased the plastic viscosity $_{C_{SS}}$  to 0.0379 Pa·s in the slurry with a GO concentration of 0.06%. The flow limit $_{HB}$  at the highest concentration of GO, equal to 0.06%, was 31.39 Pa. The coefficient of consistency $_{HB}$  in the sample with 0.06% GO concentration was  $37.27 \text{ Pa}\cdot\text{s}^n$ . Moreover, the apparent viscosity went up in sample No. 4 and was 0.098 Pa·s. When analyzing the graph of shear stress versus shear rate (Figure 1), the flow curve for slurry No. 4, containing 0.06% GO, had the highest course. Further, on the graph of apparent viscosity change versus shear rate (Figure 2), the curve for slurry No. 4 was situated highest.

Recipes with 2.5% latex content were the second group of analyzed slurries. Slurry No. 5 was the basic sample with latex and without a GO admixture. As Table 3 shows, this sample features the Casson viscosity of 0.0116 Pa·s, which was lower than the basic sample without latex. The flow limit $_{HB}$  of control sample No. 5 was 13.47 Pa, which was almost identical to the control sample without latex. The coefficient of consistency for sample No. 5 was  $0.7647 \text{ Pa}\cdot\text{s}^n$ , while the apparent viscosity was 0.056 Pa·s. As the graph of shear stress dependence on shear rate (Figure 3) shows, the flow curve in the basic sample No. 5 was situated lowest. Further, during the analysis of apparent viscosity change versus shear rate (Figure 4), the values of apparent viscosity featured the lowest course.

Moreover, in this group, the introduction of 0.01% graphene oxide addition to the latex slurry caused an increase in rheological parameters. As Table 3 shows, after adding 0.01% of GO to sample No. 6, the rheological parameters slightly increased: viscosity $_{C_{SS}}$  0.056 Pa·s, flow limit $_{HB}$  13.60 Pa, which was almost comparable with the control sample No. 5. The coefficient of consistency $_{HB}$  for the sample containing 0.01% GO was  $2.49 \text{ Pa}\cdot\text{s}^n$ , was just under three-times more than in the control sample. The apparent viscosity was comparable with the control sample and was 0.058 Pa·s. An increase in graphene oxide concentration in sample No. 7 to 0.03% resulted in a viscosity $_{C_{SS}}$  of 0.0147 Pa·s, while 0.06% GO resulted in the viscosity $_{C_{SS}}$  increased to the value of 0.0410 Pa·s. The flow limit $_{HB}$  after the use of 0.03% GO grew slightly, reaching  $14.39 \text{ Pa}\cdot\text{s}^n$ , while 0.06% GO in the slurry with latex increased the flow limit $_{HB}$  to  $22.66 \text{ Pa}\cdot\text{s}^n$  (Table 3). The coefficient of consistency for slurry No. 7, containing 0.03% GO, was  $11.0039 \text{ Pa}\cdot\text{s}^n$ , and the use of 0.06% GO caused an increase in the value to

14.9704 Pa·s<sup>n</sup>. The apparent viscosity in slurry No. 7 was 0.072 Pa·s, and the addition of 0.06% GO caused the obtainment of an apparent viscosity of 0.130 Pa·s. For the analysis of shear stress course versus shear rate for slurries with latex (Figure 3), the highest flow curve course was visible in the sample with a concentration of 0.06% GO. It was observed that shear stress values featured higher values in the latex slurry than in the slurry without latex. Further, the curve (Figure 4), illustrating the course of apparent viscosity versus shear rate was situated highest for sample No. 8, containing 0.06% GO.

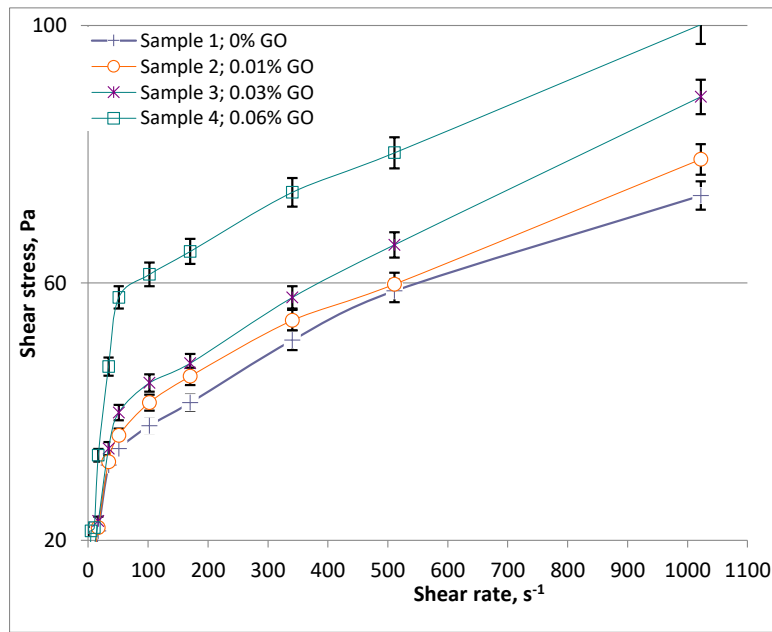


**Figure 1.** Graph of shear stress dependence on shear rate for slurries containing graphene oxide without a latex admixture.

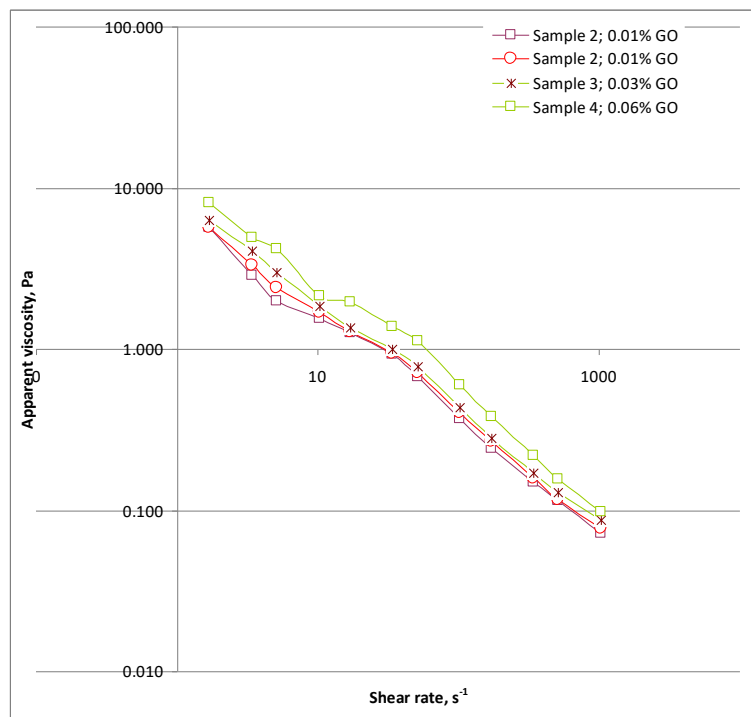


**Figure 2.** Graph of apparent viscosity change versus shear rate for slurries containing graphene oxide without a latex admixture.

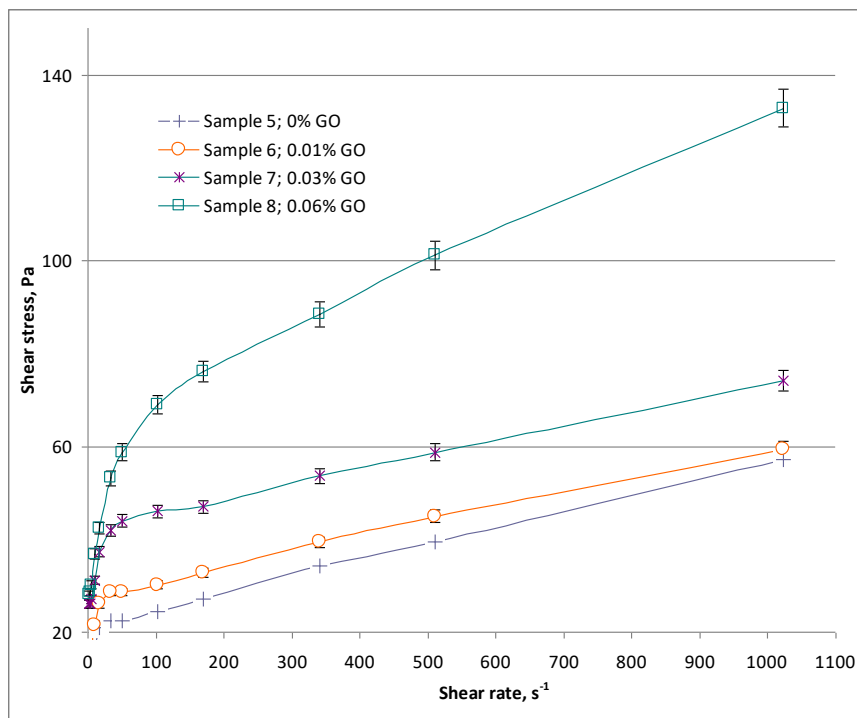


**Figure 3.** Graph of shear stress dependence on shear rate for slurries containing graphene oxide and a latex admixture.

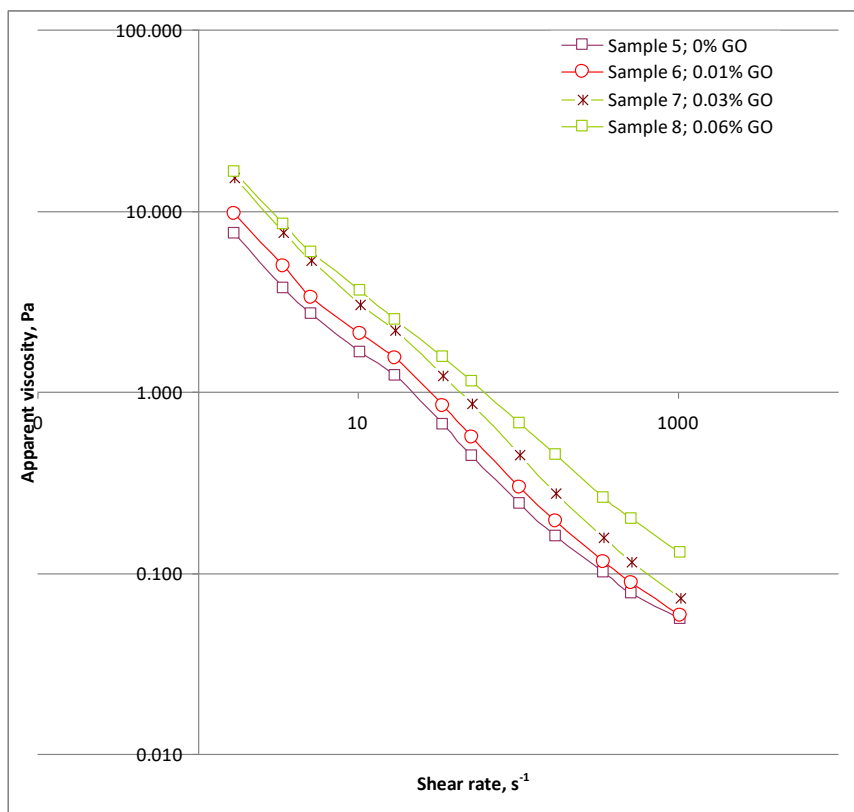


**Figure 4.** Graph of apparent viscosity change versus shear rate for slurries containing graphene oxide and a latex admixture.

As Table 4 shows, the values of apparent viscosity for slurries with graphene oxide without a latex admixture grew for each shear rate with increasing graphene oxide concentration. This resulted in the increase in a calculated apparent viscosity, which grew proportionally to the GO percentage share in the slurry. For slurries with a 2.5% latex admixture, the values of shear stress and apparent viscosity also grew proportionally to the GO share, which was visible in Table 5. However, the obtained values were higher than for the slurry without a latex admixture.

When analyzing the influence of graphene oxide on the rheological parameters of cement slurries, a regular increase in the obtained values was visible and proportional to the GO concentration. As Figure 5 shows, the increase in both viscosity<sub>CSS</sub> and apparent viscosity was small and linear for slurries without latex. While in the slurry with latex, the highest growth of apparent viscosity was visible at a GO concentration of 0.06%. The situation in the case of flow limit and coefficient of consistency described by the Herschel–Bulkley model was different. As Figure 6 shows, in the case of the slurry without a latex admixture, there was a sudden increase in the value of flow limit<sub>HB</sub> and coefficient of consistency<sub>HB</sub>. Instead, in the slurries with latex, the growth of the analyzed parameters was less sudden.

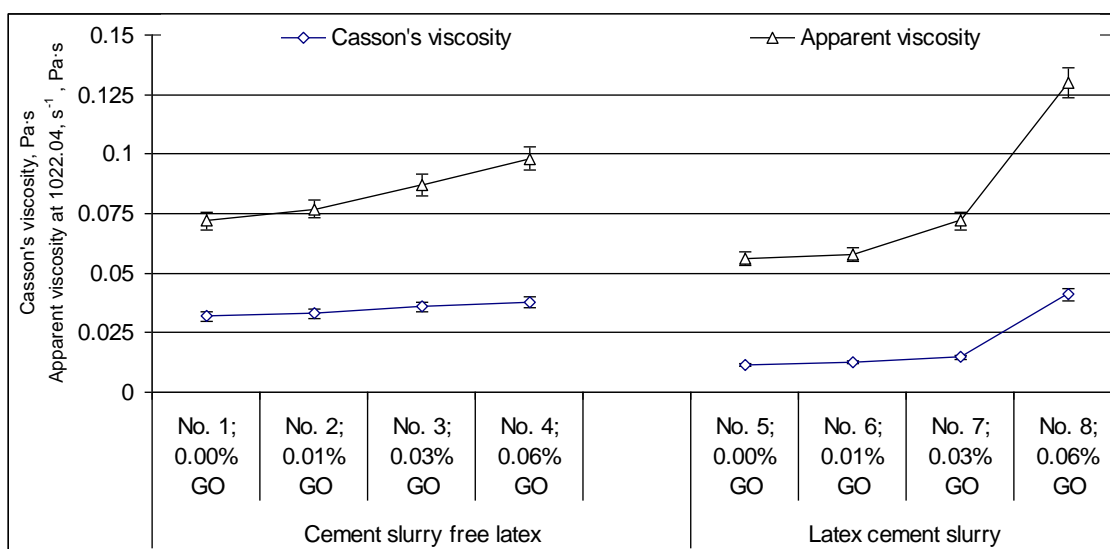


Figure 5. Casson’s viscosity and apparent viscosity change versus the graphene oxide (GO) concentration.

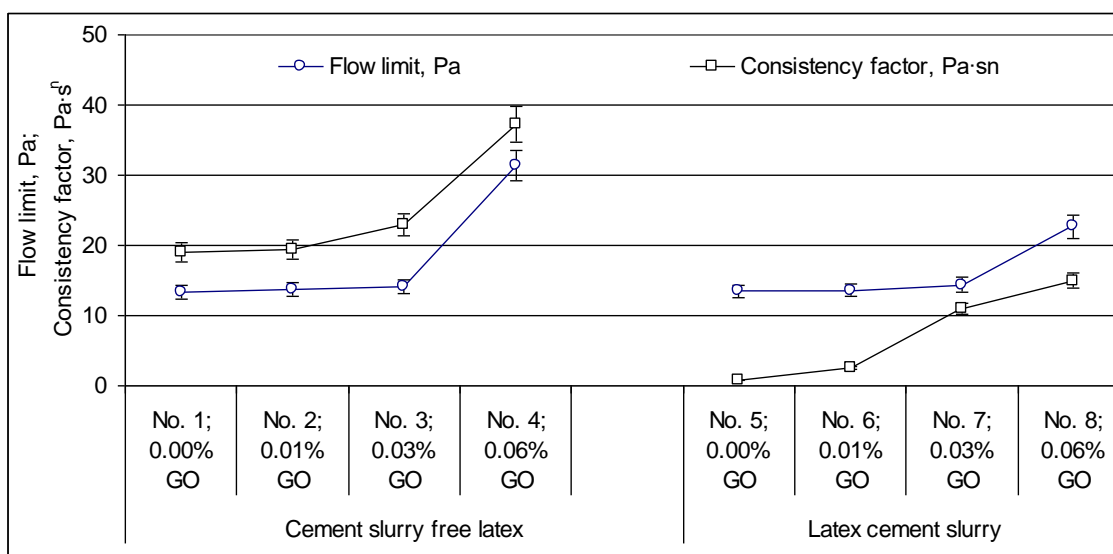


Figure 6. Flow limit and coefficient of consistency change versus the GO concentration.

#### 4. Conclusions

Because of the lack of data proving the influence of graphene oxide on the rheological parameters of cement slurries, it was necessary to carry out this research. The performed studies are useful for the drilling sector due to the possibility of determining injection expenditure and choice of pumping sets. Rheological parameters of the slurry are the main factors that decide the borehole sealing effectiveness; therefore, this was this article's focus. This was particularly important in the case of recipes with a graphene oxide admixture because such slurries provided an advanced solution for the drilling sector.

Cement slurries with a graphene oxide addition, due to their rheological properties, were best described by the Herschel–Bulkley model. Linear models, such as the Newtonian model or the Bingham model, should not be used for precise calculations of the slurry flow resistance. In such cases, the flow resistance will be burdened with a big error, especially during calculations of casing columns sealing in deep boreholes.

For the analysis of the obtained values, it was found that the graphene oxide admixture to the cement slurry resulted in an increase of its rheological parameters. The flow limit<sub>HB</sub> of the base cement slurry was 13.4 Pa and the addition of 0.01% graphene oxide increased to 13.8 Pa. The greatest increase was visible at 0.06% GO, where the flow limit<sub>HB</sub> was 31.4 Pa (Table 2). This increase was stronger in the slurries without latex. Latex slurries featured the lowest values of Casson's viscosity, apparent viscosity, flow limit<sub>HB</sub>, and plastic viscosity<sub>HB</sub>. The flow limit<sub>HB</sub> of the latex-free base cement slurry was 13.4 Pa and the base latex cement slurry was 13.5 Pa. However, after adding 0.06% GO, the latex-free cement slurry had a flow limit<sub>HB</sub> of 31.4 Pa, and the latex cement slurry had a flow limit<sub>HB</sub> of 22.6 Pa.

Casson's viscosity and apparent viscosity in the slurry with a latex admixture strongly increased after applying 0.06% of the graphene oxide concentration. Smaller GO amounts did not cause such a strong increase in the analyzed viscosity values. While in the slurry without latex, the growth of viscosity was proportional to the GO concentration and proceeded almost linearly.

The flow limit and the coefficient of consistency described by the rheological Herschel–Bulkley model suddenly increased after exceeding the 0.06% GO concentration in the slurry without latex. However, in the latex slurries, the analyzed parameters featured lower values and there was no clear increase in the value at a given GO concentration.

The lowest values of rheological parameters, among the studied slurries, featured cement slurries without a graphene oxide admixture. However, the GO admixture for concentrations ranging from 0.01% to 0.03% showed a small influence on rheological parameters. The flow limit<sub>HB</sub> was in the range of 13.4 Pa to 14.1 Pa for the latex-free cement slurry and from 13.5 Pa to 14.4 Pa for the latex cement slurry. Therefore, the concentration range of 0.01% to 0.03% GO was optimal for cement slurry technology because it caused an improvement for the slurry's mechanical parameters parallel to maintaining the rheology on the required level.

**Funding:** The work was financially supported by the Ministry of Science and Higher Education Warsaw (Internal order Oil and Gas Institute—National Research Institute Project No. 0024/KW/20 and Project No. 0096/KW/20).

**Acknowledgments:** The author thanks the anonymous reviewers for their constructive comments and the editor for handling the paper.

**Conflicts of Interest:** The author declares no conflict of interest.

## Nomenclature

Symbol	Explanation
GO	graphene oxide
GPa	gigapascal
TPa	terapascal
CSH	hydrated calcium silicates, difficult to dissolve in water
SEM	scanning electron microscopy
Ca <sup>2+</sup>	calcium cation
-COOH	carboxyl group
w/c	water–cement ratio—expresses the amount of water per cement unit
Css	the liquid described by the Casson rheological model
HB	the liquid described by the Herschel–Bulkley rheological model
$\tau$	shear stress
$\tau_y$	yield stress
$dv/dr$	shear rate gradient
$\eta$	viscosity
$\eta_{pl}$	plastic viscosity
$\eta_0$	zero viscosity
$\eta_\infty$	viscosity at the shear rate approaching infinity
k	coefficient of consistency
n	exponent
$\Phi$	degree of particles packing for the Krieger–Daugherty model
$\Phi_m$	maximum degree of packing for the Krieger–Daugherty particles
$\lambda$	time constant

## References

1. Szelać, M. *Wpływ Składu Kompozytów Cementowych na Geometrię ich Spękań Termicznych*; Politechnika Lubelska: Lublin, Poland, 2017.
2. Sun, Y.; Zhou, T.; Gao, P.; Chen, M.; Liu, H.; Xun, Y. Microstructure and Microwave Absorption Properties of Cement-Based Material Reinforced with Reduced Graphene Oxide and Nanoparticles. *Str. Mater.* **2019**, *51*, 601–608. [[CrossRef](#)]
3. Sun, S.; Han, B.; Shan, J.; Yu, X.; Wang, Y.; Li, H.; Ou, J. Nano graphite platelets-enabled piezoresistive cementitious composites for structural health monitoring. *Constr. Build. Mater.* **2017**, *136*, 314–328. [[CrossRef](#)]
4. Urban, J.; Dabrowski, P.; Binder, J.; Kopciuszynski, M.; Wysmolek, A.; Klusek, Z.; Jaloehowski, M.; Strupinski, W.; Baranowski, J. Nitrogen doping of chemical vapor deposition grown graphene on 4H-SiC (0001). *J. Appl. Phys.* **2014**, *115*, 233504. [[CrossRef](#)]
5. Zhu, Y.; Murali, S.; Cai, W.; Li, X.; Suk, J.; Potts, J.; Ruoff, R. Graphene and graphene oxide: Synthesis, properties and applications. *Adv. Mater.* **2010**, *20*, 1–19. [[CrossRef](#)]
6. Klimek-McDonald, D.; King, J.; Mikioglu, I.; Odegard, G. Mechanical properties of graphene nanoplatelet/epoxy composites. *J. Comp. Mater.* **2015**, *49*, 659–668. [[CrossRef](#)]
7. Kuila, T.; Bhadra, S.; Yao, D.; Kim, N.; Bose, S.; Lee, J. Recent Advances in Graphene Based Polymer Composites. *Prog. Polym. Sci.* **2010**, *35*, 1350–1375. [[CrossRef](#)]
8. Garg, R.; Dutta, N.; Roy Choudhury, N. Work Function Engineering of Graphene. *Nanomaterials* **2014**, *4*, 267–300. [[CrossRef](#)]
9. Compton, O.; Kim, S.; Pierre, C.; Torkelson, J.; Nguyen, S. Crumpled Graphene Nanosheets as Highly Effective Barrier Property Enhancers. *Adv. Mater.* **2010**, *22*, 4759–4763. [[CrossRef](#)]
10. Xiao, X.; Zhang, G.; Ding, Y.; Wen, D. Rheological Characteristics of Molten Salt Seeded with Al<sub>2</sub>O<sub>3</sub> Nanopowder and Graphene for Concentrated Solar Power. *Energies* **2019**, *12*, 467. [[CrossRef](#)]
11. Kremieniewski, M.; Stryczek, S. Zastosowanie cementu wysokoglinowego do sporządzania zaczynów uszczelniających w technologiach wiertniczych. *Cem. Wapno Beton* **2019**, *22*, 215–226. [[CrossRef](#)]
12. Konsta, M.; Metaxa, Z.; Shah, S. Highly dispersed carbon nanotube reinforced cement based materials. *Cem. Concr. Res.* **2010**, *40*, 1052–1059. [[CrossRef](#)]

13. Konsta, M.; Metaxa, Z.; Shah, S. Multi-scale Mechanical and Fracture Characteristics and Early-Age Strain Capacity of High Performance Carbon Nanotube/Cement Nanocomposites. *Cem. Concr. Comp.* **2010**, *32*, 110–115. [[CrossRef](#)]
14. Ranjbartoreh, A.; Wang, B.; Shen, X.; Wang, G. Advanced mechanical properties of graphene paper. *J. App. Phys.* **2011**, *109*, 014306. [[CrossRef](#)]
15. Kasiralvalad, E. The great potential of nanomaterials in drilling & drilling fluid applications. *Int. J. Nano Dimens.* **2014**, *5*, 463–471.
16. Li, F.; Jiang, X.; Zhao, J.; Zhang, S. Graphene oxide: A promising Nanomaterial for energy and environmental applications. *Nano Energy* **2015**, *16*, 488–515. [[CrossRef](#)]
17. Li, G.; Wang, P.; Zhao, X. Mechanical Behavior and Microstructure of Cement Composites Incorporating Surface-Treated Multi-Walled Carbon Nanotubes. *Carbon* **2005**, *43*, 1239–1245. [[CrossRef](#)]
18. Jamrozik, A. Graphene and graphene oxide in the oil and gas industry. *AGH Drill. Oil Gas* **2017**, *34*, 731. [[CrossRef](#)]
19. Pan, Z.; He, L.; Qiu, L.; Habibnejad Korayem, A.; Li, G.; Zhu, J.; Collins, F.; Li, D.; Duan, W.; Wang, M. Mechanical properties and microstructure of a graphene oxide-cement composite. *Cem. Conc. Comp.* **2015**, *58*, 140–147. [[CrossRef](#)]
20. Almalkawi, A.T.; Salem, T.; Hamadna, S.; Darsanasiri, A.G.N.D.; Soroushian, P.; Balchandra, A.; Al-Chaar, G. Physio-Microstructural Properties of Aerated Cement Slurry for Lightweight Structures. *Materials* **2018**, *11*, 597. [[CrossRef](#)]
21. Kremieniewski, M. Ultra-Lightweight Cement Slurry to Seal Wellbore of Poor Wellbore Stability. *Energies* **2020**, *13*, 3124. [[CrossRef](#)]
22. Sun, Y.; Chen, M.; Gao, P.; Zhou, T.; Liu, H.; Xun, Y. Microstructure and microwave absorbing properties of reduced graphene oxide/Ni/multi-walled carbon nanotubes/Fe<sub>3</sub>O<sub>4</sub> filled monolayer cement-based absorber. *Adv. Mech. Eng.* **2019**, *11*, 168781401882288. [[CrossRef](#)]
23. Sedaghat, A.; Ram, M.; Zayed, A.; Kamal, R.; Shanahan, N. Investigation of Physical Properties of Graphene-Cement Composite for Structural Applications. *J. Comp. Mater.* **2014**, *4*, 12–21. [[CrossRef](#)]
24. Makar, J.; Margeson, J.; Luh, J. Carbon nanotube/cement composites—early results and potential applications. In Proceedings of the 3rd International Conference on Construction Materials: Performance, Innovations and Structural Implications, Vancouver, BC, Canada, 22–24 August 2005.
25. Kremieniewski, M. Recipe of Lightweight Slurry with High Early Strength of the Resultant Cement Sheath. *Energies* **2020**, *13*, 1583. [[CrossRef](#)]
26. Tao, C.; Kutchko, B.G.; Rosenbaum, E.; Wu, W.-T.; Massoudi, M. Steady Flow of a Cement Slurry. *Energies* **2019**, *12*, 2604. [[CrossRef](#)]
27. Kędzierski, M.; Rzepka, M.; Kremieniewski, M. Możliwości zastosowania nanorurek węglowych (CNTs) w technologii zaczynów cementowych. *Nafta-Gaz* **2020**, *2*, 110–118. [[CrossRef](#)]
28. Kremieniewski, M. Zmiana wczesnej wytrzymałości na ściskanie pod wpływem wybranych środków poprawiających stabilność sedymentacyjną. *Nafta-Gaz* **2020**, *7*, 466–473. [[CrossRef](#)]
29. Laila, R.; James, B.; Alizadeh, A.; Jon, M.; Taijiro, S. Cement and Concrete Nanoscience and Nanotechnology. *Materials* **2010**, *3*, 918–942. [[CrossRef](#)]
30. Jialin, Y.; Wang, S.; Kim, J. Preparation of graphite nanoplatelets and graphene sheets. *J. Coll. Int. Sci.* **2009**, *336*, 592–598. [[CrossRef](#)]
31. Saafi, M.; Tang, L.; Fung, J.; Rahman, M.; Liggat, J. Enhanced Properties of Graphene/Fly Ash Geopolymeric Composite Cement. *Cem. Concr. Res.* **2015**, *67*, 292–299. [[CrossRef](#)]
32. Babak, F.; Hassani, A.; Rashidi, A.; Parviz, G. Preparation and Mechanical Properties of Graphene Oxide: Cement Nanocomposites. *Sci. World J.* **2014**, *2014*, 276323. [[CrossRef](#)]
33. Layek, R.; Nandi, A. A review on synthesis and properties of polymer functionalized graphene. *Polymer* **2013**, *54*, 5087–5103. [[CrossRef](#)]
34. Ahmed, A.; Mahmoud, A.A.; Elkatatny, S.; Chen, W. The Effect of Weighting Materials on Oil-Well Cement Properties While Drilling Deep Wells. *Sustainability* **2019**, *11*, 6776. [[CrossRef](#)]
35. Niu, J.; Wang, B.; Feng, C.; Chen, K. Experimental Research on Viscosity Characteristics of Grouting Slurry in a High Ground Temperature Environment. *Materials* **2020**, *13*, 3221. [[CrossRef](#)] [[PubMed](#)]
36. Kremieniewski, M. Zaczyny do uszczelniania otworów w warunkach niskich wartości gradientów ciśnienia szczelinowania skał oraz do prac rekonstrukcyjnych. *Nafta-Gaz* **2020**, *76*, 102–109. [[CrossRef](#)]

37. Glukharev, A.; Konakov, V. Synthesis and Properties of Zirconia-Graphene Composite Ceramics: A Brief Review. *Rev. Adv. Mater. Sci.* **2018**, *56*, 124–138. [[CrossRef](#)]
38. Kremieniewski, M.; Stryczek, S.; Wiśniowski, R.; Gonet, A. Zmniejszanie porowatości stwardniałych zaczynów wiertniczych poprzez wprowadzenie dodatków drobnoziarnistych. *Cem. Wapno Beton* **2016**, *21*, 325–335.
39. Qin, D.; Liu, Z.; Sun, D.; Song, X.; Bai, H. A new nanocomposite forward osmosis membrane custom-designed for treating shale gas wastewater. *Sci. Rep.* **2015**, *5*, 14530. [[CrossRef](#)]
40. Yang, H.; Cui, H.; Tang, W.; Li, Z.; Han, N.; Xing, F. A Critical Review on Research Progress of Graphene/Cement Based Composites. *Compos. Part A App. Sci. Manuf.* **2017**, *102*, 273–296. [[CrossRef](#)]
41. Richhariya, G.; Dora, D.; Parmar, K.; Pant, K.; Singhal, N.; Lal, K.; Kundu, P. Development of Self-Healing Cement Slurry through the Incorporation of Dual-Encapsulated Polyacrylamide for the Prevention of Water Ingress in Oil Well. *Materials* **2020**, *13*, 2921. [[CrossRef](#)]
42. Kremieniewski, M. Wpływ perlitu pylistego na własności technologiczne zaczynu cementowego. *Nafta-Gaz* **2017**, *12*, 943–952. [[CrossRef](#)]
43. Stryczek, S.; Wiśniowski, R.; Gonet, A.; Złotkowski, A. Wpływ rodzaju cementu na właściwości reologiczne zaczynów uszczelniających stosowanych w technologiach wiertniczych. *Wiert. Naft. Gaz.* **2010**, *27*, 721–739.
44. Tao, C.; Kutchko, B.G.; Rosenbaum, E.; Massoudi, M. A Review of Rheological Modeling of Cement Slurry in Oil Well Applications. *Energies* **2020**, *13*, 570. [[CrossRef](#)]
45. Kremieniewski, M. Korelacja wyników badań wytrzymałości na ściskanie i przyczepności do rur stalowych płaszczka cementowego z zaczynu o obniżonej gęstości. *Nafta-Gaz* **2019**, *10*, 613–624. [[CrossRef](#)]
46. E Silva, R.A.; Guetti, P.; Luz, M.; Rouxinol, F.; Gelamo, R. Enhanced properties of cement mortars with multilayer graphene nanoparticles. *Constr. Build. Mater.* **2017**, *149*, 378–385. [[CrossRef](#)]
47. Czarnecki, L. Nanotechnologia w budownictwie. *Przegl. Bud.* **2011**, *1*, 40–53.
48. Bong, J.; Lim, T.; Seo, K.; Kwon, C.; Park, J.; Kwak, S.; Ju, S. Dynamic graphene filters for selective gas-water-oil separation. *Sci. Rep.* **2015**, *5*, 14321. [[CrossRef](#)]
49. Konios, D.; Stylianakis, M.; Stratakis, E.; Kymakis, E. Dispersion behavior of graphene oxide and reduced graphene oxide. *J. Coll. Int. Sci.* **2014**, *430*, 108–112. [[CrossRef](#)]
50. Wang, Z.; Han, F.; Ji, Y.; Li, W. Performance and Exergy Transfer Analysis of Heat Exchangers with Graphene Nanofluids in Seawater Source Marine Heat Pump System. *Energies* **2020**, *13*, 1762. [[CrossRef](#)]
51. Pasquini, L. Design of Nanomaterials for Hydrogen Storage. *Energies* **2020**, *13*, 3503. [[CrossRef](#)]
52. Kremieniewski, M. Wpływ drobnoziarnistej krzemionki na parametr czasu oczekiwania na cement—WOC. *Nafta-Gaz* **2019**, *75*, 683–690. [[CrossRef](#)]
53. Potts, J.; Dreyer, D.; Bielawski, C.; Ruoff, R. Graphene-Based Polymer Nanocomposites. *Polymer* **2011**, *52*, 5–25. [[CrossRef](#)]
54. Zhang, S.; Sun, J.; Zhang, X.; Xin, J.; Miao, Q.; Wang, J. Chemical Society Reviews. *Chem. Soc. Rev.* **2014**, *43*, 7838–7869. [[CrossRef](#)] [[PubMed](#)]
55. Bentz, D.; Garboczi, E.; Haecker, C.; Jensen, O. Effects of Cement Particle Size Distribution on Performance Properties of Portland Cement-Based Materials. *Cem. Concr. Res.* **1999**, *29*, 1663–1671. [[CrossRef](#)]
56. Khan, N.S.; Gul, T.; Kumam, P.; Shah, Z.; Islam, S.; Khan, W.; Zuhra, S.; Sohail, A. Influence of Inclined Magnetic Field on Carreau Nanoliquid Thin Film Flow and Heat Transfer with Graphene Nanoparticles. *Energies* **2019**, *12*, 1459. [[CrossRef](#)]
57. Kremieniewski, M. Zmiana parametrów reologicznych zaczynu lateksowego pod wpływem dodatku mikrosfery. *Nafta-Gaz* **2020**, *76*, 37–45. [[CrossRef](#)]
58. Huczko, A. Fulereny i nanorurki. *Academia* **2006**, *2*, 16.
59. Lavrov, A.; Todorovic, J.; Torsæter, M. Impact of Voids on Mechanical Stability of Well Cement. *Energy Proced.* **2016**, *86*, 401–410. [[CrossRef](#)]
60. Chen, J.; Zhao, D.; Ge, H.; Wang, J. Graphene oxide-deposited carbon fiber/cement composites for electromagnetic interference shielding application. *Constr. Build. Mater.* **2015**, *84*, 66–72. [[CrossRef](#)]
61. Mahmoud, A.A.; Elkatatny, S.; Ahmed, A.; Gajbhiye, R. Influence of Nanoclay Content on Cement Matrix for Oil Wells Subjected to Cyclic Steam Injection. *Materials* **2019**, *12*, 1452. [[CrossRef](#)]
62. Kremieniewski, M. Lekkie zaczyny cementowe do uszczelniania technicznych kolumn rur okładzinowych. *Nafta-Gaz* **2010**, *66*, 477–480.

63. Prabakaran, R.; Sidney, S.; Lal, D.M.; Selvam, C.; Harish, S. Solidification of Graphene-Assisted Phase Change Nanocomposites inside a Sphere for Cold Storage Applications. *Energies* **2019**, *12*, 3473. [[CrossRef](#)]
64. Natarajan, S.; Rajasekar, R.; Mahalakshmi, S.; Sathishkumar, T.; Sasikumar, K.; Sahoo, S. Graphene and modified graphene-based polymer nanocomposites—A review. *J. Rein. Plast. Comp.* **2014**, *33*, 1158–1170. [[CrossRef](#)]
65. Joshi, R.; Carbone, P.; Wang, F.; Kravets, V.; Su, Y.; Grigorieva, I.; Wu, H.; Geim, A.; Raveendran-Nair, R. Precise and Ultrafast Molecular Sieving Through Graphene Oxide Membranes. *Science* **2015**, *343*, 752–754. [[CrossRef](#)] [[PubMed](#)]
66. Thalib, M.M.; Manokar, A.M.; Essa, F.A.; Vasimalai, N.; Sathyamurthy, R.; Garcia Marquez, F.P. Comparative Study of Tubular Solar Stills with Phase Change Material and Nano-Enhanced Phase Change Material. *Energies* **2020**, *13*, 3989. [[CrossRef](#)]
67. Chandrasekaran, S.; Sato, N.; Tölle, F.; Mülhaupt, R.; Fiedler, B.; Karl, S. Fracture toughness and failure mechanism of graphene based epoxy composites. *Comp. Sci. Technol.* **2014**, *97*, 90–99. [[CrossRef](#)]
68. Berman, D.; Erdemir, A.; Sumant, A. Few layer graphene to reduce wear and friction on sliding steel surfaces. *Carbon* **2012**, *54*, 454. [[CrossRef](#)]
69. Hartmann, S.J.; Iurchenkova, A.A.; Kallio, T.; Fedorovskaya, E.O. Electrochemical Properties of Nitrogen and Oxygen Doped Reduced Graphene Oxide. *Energies* **2020**, *13*, 312. [[CrossRef](#)]

**Publisher’s Note:** MDPI stays neutral with regard to jurisdictional claims in published maps and institutional affiliations.



© 2020 by the author. Licensee MDPI, Basel, Switzerland. This article is an open access article distributed under the terms and conditions of the Creative Commons Attribution (CC BY) license (<http://creativecommons.org/licenses/by/4.0/>).